Structural and transport properties of neutral radical crystals of $Co^{III}(tmp)(CN)_2$ (tmp = 5,10,15,20-tetramethylporphyrinato) and the CN-bridged polymer of $[Co^{III}(tmp)(CN)]_n$†

Masashi Kurokawa,[a] Judy Fe F. Jose-Larong,[b,‡] Hiroyuki Hasegawa,[c] Yukihiro Takahashi,[a,b,c] Jun Harada[a,b,c] and Tamotsu Inabe*[,a,b,c]

[a]*Graduate School of Chemical Sciences and Engineering, Hokkaido University, Sapporo 060-0810, Japan,*

[b]*Department of Chemistry, Graduate School of Science, Hokkaido University, Sapporo 060-0810, Japan*

[c]*Department of Chemistry, Faculty of Science, Hokkaido University, Sapporo 060-0810, Japan. E-mail: inabe@sci.hokudai.ac.jp*

†Electronic supplementary information (ESI) available. CCDC 1518172–1518175. Crystallographic data in CIF for TPP[Co(tmp)$(CN)_2$]·1/2(acetone)·H_2O, {[Co(tmp)(CN)](acetone)}$_n$, Co(tmp)$(CN)_2$, and Co(tmp)$(CN)_2$·2CH_3CN. Powder diffraction of Co(tmp)$(CN)_2$. Cyclic voltammetry of TPP[Co(tmp)$(CN)_2$]. ESR spectrum of Co(tmp). For ESI and crystallographic data in CIF or other electronic format see DOI: 10.1039/XXXXXXX.

‡Present address: Ontario International College, 4620 Finch Avenue East, Toronto, Ontario M1S 4G2, Canada

Abstract

An axially ligated Co(tmp) (tmp = 5,10,15,20-tetramethylporphyrinato) anion, $[Co^{III}(tmp)(CN)_2]^-$, has been prepared and subjected to electrochemical oxidation to make the tmp π-ligand open shell. With acetone as the solvent, solvent-free neutral radical crystals of $Co^{III}(tmp)(CN)_2$ are obtained, whereas solvent-inclusive crystals of $Co^{III}(tmp)(CN)_2 \cdot 2CH_3CN$ are obtained with CH_3CN as the solvent. In both crystals, the open shell tmp ring deforms into a ruffled form, which makes the π–π interactions in the crystal weak. Thus, the electrical conductivity is low, and the crystals behave as semiconductors with room temperature resistivity of 10^6 Ω cm and an activation energy of about 0.3 eV. When the solvent is acetone, non-oxidized crystals of the CN-bridged polymer $\{[Co^{III}(tmp)(CN)](acetone)\}_n$ are obtained as a byproduct. The closed shell tmp ring deforms into a ruffled form, and there π–π interactions in the crystal are negligible. The room temperature resistivity is rather high at about 10^8 Ω cm.

INTRODUCTION

Phthalocyanine (Pc) is a macrocyclic π-conjugated ligand, and its metal complexes are well known as dyes with various electronic functionalities.[1] Many studies have investigated the electrical functionalities of these dyes. Charge transport in single crystals and thin films was initially studied about 50 years ago.[2] The conductivity obtained in earlier studies was not high because the Pc ligand was in a closed shell form. Metallic conduction was realized by partial oxidation of the Pc ring in 1980, and this led to the recognition of these dyes as good conductors.[3] Since then, many Pc conductors have been reported.[4] While many of them are one-dimensional conductors composed of face-to-face stacked planar Pc molecules, we have reported highly conducting crystals of axially ligated Pc compounds ($M(Pc)X_2$ with X = CN, Cl, and Br; Fig. 1a).[5-9] When M was Fe^{III}, the partially oxidized conductors showed giant negative magnetoresistance because of the interaction between the π-ligand-based conduction electrons and d-centered magnetic moments (π-d interaction, Fig. 1b).[10,11] Currently, elucidation of the detailed mechanism is still in progress. However, an approximate mechanism for the generation of the negative magnetoresistance effects is detailed below. Generally, in the axially ligated system, overlap between the Pc rings is reduced, resulting in narrowing of the conduction band originating from the π–π interaction. This situation makes the system susceptible to electron correlation, resulting in charge disproportionation in the ground state.[12] In the Fe system, conduction electrons are more localized because of the π-d interaction, and short-range antiferromagnetic ordering of the localized Fe-centered d-spins occurs through the π-d interaction.[13] External magnetic fields break this order and release the conduction π-electrons from the localized state.

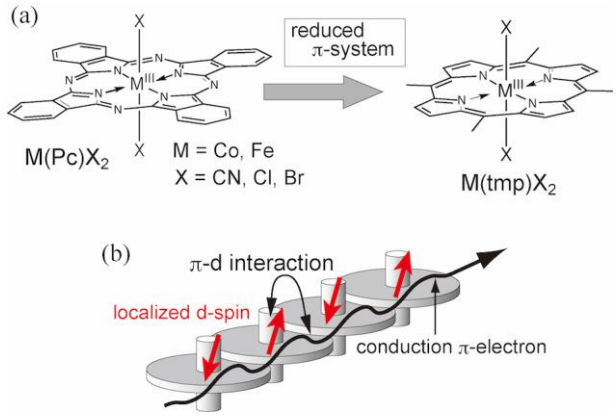

Fig. 1 (a) Axially ligated Pc and tmp complexes. (b) Schematic of the Pc π-d

system with M = Fe.

There are many factors associated with the negative magnetoresistance. Among these factors, an important one is electron correlation. Because each $M(Pc)X_2$ unit formally bears a 1/2 hole in the conductors (e.g., the composition is $A[M(Pc)X_2]_2$, where A is a closed-shell cation), the conduction band is 3/4-filled, which leads to the metallic state. However, the charge transport shows thermally activated behavior because of the charge disproportionation even without localized d-spins.[12] If one could increase the electron correlation, localization of the conduction electrons would be more developed. Such a situation is expected to increase the temperature at which negative magnetoresistance effects appear for the system with magnetic moments.

Reduction of the π-conjugation size is considered a promising approach to increase the electron correlation. The porphyrin ring, which does not have the periphery benzo rings of Pc, is a candidate for this. The meso C-H groups in the original porphyrin ring have to be protected because of their high reactivity. As the smallest substituents that will not interfere with the intermolecular π–π interaction for the axially ligated form, four methyl groups are introduced (Fig. 1a). Thus, we prepared an axially ligated anionic complex of 5,10,15,20-tetramethylporphyrinato (tmp). For the planar complex of Ni(tmp), face-to-face stacked one-dimensional conductors have been reported.[14-16] Therefore, the tmp ring itself is a promising macrocycle to obtain conducting partially oxidized salts. As a first step, we selected Co^{III} as a central metal ion, because it is a non-magnetic innocent ion under strong octahedral coordination circumstances with axial CN ligands. We synthesized $[Co^{III}(tmp)(CN)_2]^-$, and subjected it to electrochemical oxidation to make the π-ligand open shell. In this paper, we describe the synthesis of the starting anionic tmp complex, cation exchange by metathesis, and electrocrystallization. We discuss the crystal structures of the starting complex and the products, and their physical properties. In the course of this study, we also obtained single crystals of the CN-bridged polymer. To date, there have been no reports of the detailed structural properties of this type of a one-dimensional polymer. We disclose the single-crystal structural and physical properties of the porphyrin-based CN-bridged polymer in this paper.

Experimental section

Materials

H_2(tmp). Using an established method,[17] 8.4 mL of pyrrole (TCI Co. Ltd., Tokyo, Japan) was reacted with 2.6 mL of 99.5 % acetaldehyde (Sigma-Aldrich, St. Louis, MO) in a pre-heated (85–88 °C) mixture of 500 mL of propionic acid (TCI Co. Ltd.), 24 mL of water, and 2 mL of pyridine (Wako Pure Chemical Industries, Ltd., Osaka, Japan). After 30 min, another 1.0 mL of acetaldehyde was added to the reaction mixture and the mixture was stirred continually for another 2 h at 85–88 °C. After this time, the mixture was cooled to room temperature and a shiny purple precipitate appeared. The precipitate was isolated by filtration, washed with methanol, and dried under vacuum. The yield was about 4%. This low yield was thought to be caused by oligomerization of the reagents.

Co^{II}(tmp). Co(tmp) was prepared following an established procedure[18] with some modifications. About 200 mg of the synthesized H_2(tmp) was dissolved in dehydrated dimethylformamide and 240 mg of anhydrous $Co(OAc)_2$ was added. The mixture was allowed to undergo reflux for 6–8 h under an Ar atmosphere. Completion of the reaction was monitored by thin layer chromatography and ultraviolet-visible spectroscopy. The reaction mixture was cooled to room temperature and then put in an ice water bath to allow a dark crystalline precipitate to form. The precipitate was isolated by filtration and washed with cold water, methanol, and hexane consecutively. The product was purified by vacuum sublimation. The yield was about 60%.

Na[Co^{III}(tmp)$(CN)_2$]. First, 160 mg of Co(tmp) in 50 mL of tetrahydrofuran (Wako Pure Chemical Industries, Ltd.) was combined with 0.38 g of sodium cyanide (Wako Pure Chemical Industries, Ltd.) in 7 mL of water. The resulting solution was mixed overnight.[19] Then, 100 mL of chloroform was added to the mixture in an ice water bath. A green fine precipitate formed and was isolated by filtration, and washed with chloroform. The yield was about 70%.

Tetraphenylphosphonium[Co^{III}(tmp)$(CN)_2$]·1/2(acetone)·H_2O. An excess (ca. 2.5 molar excess) of tetraphenylphosphonium (TPP) iodide was added to 10 mg of Na[Co(tmp)$(CN)_2$] in acetone. After 5–7 days of evaporation of the solvent, large dark platelet crystals of the TPP salt were obtained. The crystals were submitted to X-ray crystallography, and the final composition was determined to be TPP[Co(tmp)$(CN)_2$]·1/2(acetone)·H_2O. The composition was consistent with the elemental analysis: Found, C: 71.91%, H: 5.14%, N: 9.77%; Calcd. for

TPP[Co(tmp)$(CN)_2$]·1/2(acetone)·H_2O, C: 71.76%, H: 5.26%, N: 9.75%.

Co^{III}(tmp)$(CN)_2$. Electrolysis of TPP[Co(tmp)$(CN)_2$]·1/2(acetone)·H_2O in acetone under N_2 with a constant current of 2 μA at 20 °C yielded small bluish-black neutral radical crystals of Co^{III}(tmp)$(CN)_2$ on the anode surface within 5 days. For the electrolysis, a solution of 15 mg of the TPP salt in about 30 mL of acetone was placed in a two-compartment electrocrystallization cell divided by a glass frit without any supporting electrolyte. A platinum wire electrode (1 mm in diameter and about 30 mm in length) was immersed in each compartment, and a current flowed between the two electrodes. The yield of the crystals was low (typically 10%). Among the crystals harvested, relatively large ones were submitted to X-ray crystallography and transport measurements. The microcrystalline product was used for optical and electron spin resonance (ESR) measurements. In order to identify the microcrystalline product as Co^{III}(tmp)$(CN)_2$, powder diffraction measurement was performed (Fig. S1 in the ESI†).

Co^{III}(tmp)$(CN)_2$·2CH_3CN. Electrolysis of TPP[Co(tmp)$(CN)_2$]·1/2(acetone)·H_2O in highly anhydrous CH_3CN under N_2 with a constant current of 2–3 μA at 15 °C yielded a small amount of bluish-black neutral radical crystals of Co^{III}(tmp)$(CN)_2$·2CH_3CN on the anode surface within 5 days. The procedures and apparatus were the same as those adopted for the electrocrystallization of Co^{III}(tmp)$(CN)_2$. A few relatively large crystals were submitted to X-ray crystallography and transport measurements.

{[Co^{III}(tmp)(CN)](acetone)}$_n$. In addition to the neutral radical crystals grown in the liquid phase, when TPP[Co(tmp)$(CN)_2$]·1/2(acetone)·H_2O was left in the acetone solution for electrolysis, a small amount of dark blue needle-like crystals grew near the liquid-vapor boundary on the electrode. X-ray crystallography indicated that the crystals were CN-bridged polymer [Co^{III}(tmp)(CN)]$_n$ and contained the solvent. The valence of each component indicates that the tmp ligand is not oxidized. It was easy to distinguish the polymer crystals from the neutral radical crystals by their appearance.

Crystal structure analyses

X-ray crystallography was performed on a Bruker SMART APEX II ULTRA diffractometer with a turbo X-ray source rotating anode (Mo Kα radiation, λ = 0.71073 Å) and multilayer optics. Data collection was performed using a Japan Thermal Engineering DX-CS190LD N_2 gas-flow cryostat. The structures were solved by direct

methods (SHELXT-2014) and refined by full-matrix least-squares on F^2 using SHELXL-2014.[20] All H atoms were refined using riding models. For crystals without disorders, all non-H atoms were refined anisotropically. The crystal and experimental data are summarized in Table 1.

Table 1 Crystallographic data for TPP[Co(tmp)$(CN)_2$]·1/2(acetone)·H_2O, {[Co(tmp)(CN)](acetone)}$_n$, Co(tmp)$(CN)_2$, and Co(tmp)$(CN)_2$·2CH_3CN

	TPP[Co(tmp)$(CN)_2$]·1/2(acetone)·H_2O	{[Co(tmp)(CN)](acetone)}$_n$	Co(tmp)$(CN)_2$	Co(tmp)$(CN)_2$·2CH_3CN
formula	$C_{51.5}H_{45}N_6O_{1.5}PCo$	$C_{28}H_{26}N_5OCo$	$C_{26}H_{20}N_6Co$	$C_{30}H_{26}N_8Co$
formula weight	861.83	507.47	475.41	557.52
crystal size (mm^3)	0.29 × 0.12 × 0.05	0.13 × 0.04 × 0.04	0.13 × 0.07 × 0.03	0.12 × 0.08 × 0.03
crystal system	triclinic	monoclinic	triclinic	monoclinic
space group	*P*-1	$P2_1$	*P*-1	*C*2/*c*
a (Å)	12.0125(9)	11.7053(17)	8.6078(17)	12.9104(16)
b (Å)	13.6844(10)	19.130(3)	9.3943(18)	14.7785(18)
c (Å)	14.8622(11)	11.7373(17)	13.337(3)	14.7219(18)
α (deg)	65.6430(10)	90	89.409(4)	90
β (deg)	69.3160(10)	114.655(2)	81.068(4)	114.3679(18)
γ (deg)	77.5240(10)	90	76.910(3)	90
V ($Å^3$)	2075.1(3)	2388.7(6)	1037.3(4)	2558.7(5)
Z	2	4	2	4
T (K)	100	100	100	110
no. of reflns collected	40176	52132	30578	18456
no. of independent reflns	9517	11380	4755	2951
R_{int}	0.0182	0.0985	0.0867	0.0299
goodness-of-fit on F^2	1.047	1.084	1.056	1.114
R_1 [$I > 2\sigma(I)$]	0.0372	0.0698	0.0612	0.0372
R_w (all data)	0.1022	0.1581	0.1408	0.0993

Measurements and calculations

Electrical resistivity was measured for a single crystal or a compacted pellet using a two-probe method. Diffuse reflectance visible–near-infrared spectra were recorded on a JASCO V-570 spectrometer by diluting the sample in KBr powder. The reflectance spectra were converted to the Kubelka-Munk function. Fourier transform infrared spectra were measured by a Perkin Elmer Spectrum One spectrometer using KBr pellet samples. ESR measurements were performed for Co^{II}(tmp), TPP[Co^{III}(tmp)$(CN)_2$]·1/2(acetone)·H_2O, and Co^{III}(tmp)$(CN)_2$ using a Bruker X-band EMX081S spectrometer. Randomly oriented microcrystalline samples were used for the measurements. Receiver gain and modulation amplitude for Co^{III}(tmp)$(CN)_2$ and the TPP salt were 10^3 and 1.00 G, respectively. Powder X-ray diffraction patterns were measured using a Bruker D8 ADVANCE diffractometer. Cyclic voltammograms were obtained using a Hokuto Denko Hz 3000 Automatic Polarization System. The reference electrode was Ag/AgCl. The overlap integrals between singly occupied molecular orbitals (SOMOs), SOMO-highest occupied molecular orbital (HOMO), and HOMOs of the tmp ligands were calculated using atomic parameters determined by the X-ray analyses using the CAESAR program package.[21]

Results and discussion

Structures of crystals with closed shell tmp ligands

TPP[Co(tmp)$(CN)_2$]·1/2(acetone)·H_2O. TPP^+ and $[Co(tmp)(CN)_2]^-$ are arranged alternately, and there is a weak π–π interaction between $[Co(tmp)(CN)_2]^-$ anions (Fig. 2). The tmp ligand is deformed into a ruffled form with two of the methyl groups oppositely arranged pointing upward and the other two downward. The crystal contains solvent molecules and the composition is TPP^+:$[Co(tmp)(CN)_2]^-$:acetone:H_2O = 2:2:1:2.

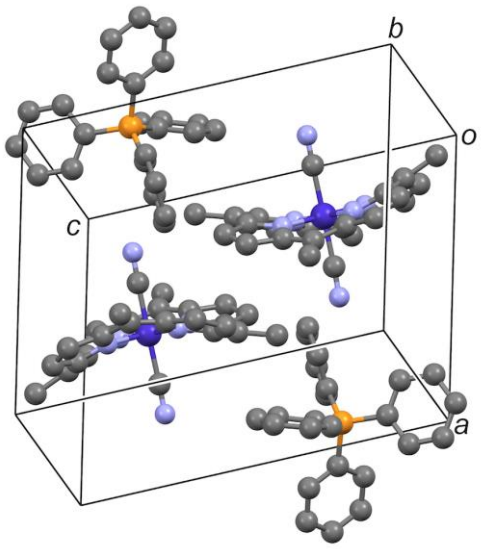

Fig. 2 Perspective view of the unit cell of TPP[Co(tmp)$(CN)_2$]·1/2(acetone)·H_2O (for clarity, acetone and H_2O are omitted).

{[Co(tmp)(CN)](acetone)}$_n$. The two Co(tmp)CN units are crystallographically independent. Both tmp ligands are closed shell, and deformed into the ruffled form. The connection order is ···Co–CN–Co–CN–Co··· (Co–C bond length: 1.87–1.88 Å, Co–N bond length: 1.94 Å. Possibility of the CN/NC disorder is negligible). Along the polymer chain, there are 2_1 screw axes, and the polymer chain becomes helical. The crystal contains solvent molecules, and they occupy the space between the tmp rings in the chain (Fig. 3). The Pc analogs, [M(Pc)CN]$_n$, were widely studied by Hanack, et al.,[22,23] but the crystal structure was not clarified. The crystal structure of the dimeric system of (CN)Co(Pc)–CN–Co(Pc)(CN) has been reported.[24] In this case, the Pc rings in the dimer are not parallel but tilted to sandwich another π-conjugated compound between them. If this type of CN-bridged polymer with the M–CN–M length (separation between the macrocyclic π-ligands) of approximately 5.2 Å is packed with keeping the linear form, it inevitably produces unoccupied spaces between the polymer chains. Therefore, the assemblies of CN-bridged compounds are stabilized only when they contain components that occupy the separation between the two macrocycles. This brings non-linearity to the ···Co–CN–Co–CN–Co··· polymer backbone. In {[Co(tmp)(CN)](acetone)}$_n$, acetone is the component that opens up the separation between the tmp rings. The angles between the least-squares mean planes (calculated using 24 atoms in each tmp ring) in the polymer are 24.4˚ and 28.1˚. In the former, a

stationary acetone molecule is inserted (Fig. 3a), whereas in the latter, a disordered acetone is inserted (Fig. 3b). Weak π–π interactions may operate between the tilted tmp rings within the polymer chains. However, inter-polymer π–π interactions are negligible. In the Pc analog of $[M(Pc)CN]_n$, non-linear polymer chains may be assembled with partly interdigitating the Pc rings, leading to appreciable inter-polymer π–π interactions.

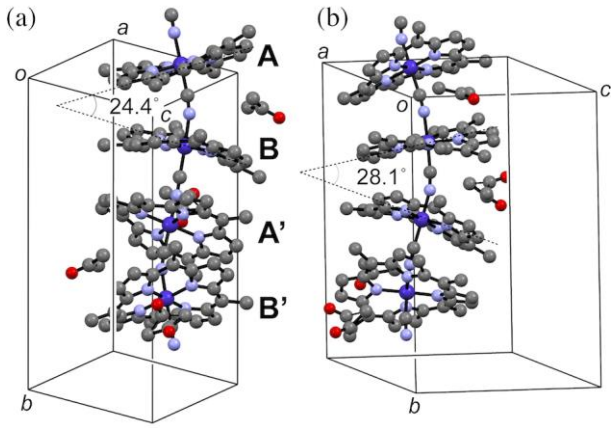

Fig. 3 $[Co(tmp)(CN)]_n$ polymer chain in $\{[Co(tmp)(CN)](acetone)\}_n$; (a) showing acetone insertion between the rings A and B, and (b) showing acetone insertion between the rings B and A'.

Molecular structure of the closed shell tmp. The tmp rings in both TPP salt and CN-bridged polymer have the ruffled conformation. The average values of the absolute distances from the least-squares mean plane to the meso carbons are 0.68 Å in $TPP[Co(tmp)(CN)_2]\cdot 1/2(acetone)\cdot H_2O$ and 0.54 Å and 0.51 Å in the CN-bridged polymer (Fig. 4). The reduced deformation in the CN-bridged polymer may be caused by the structural features of the polymer, namely crystallization with insertion of solvent molecules between the tmp rings.

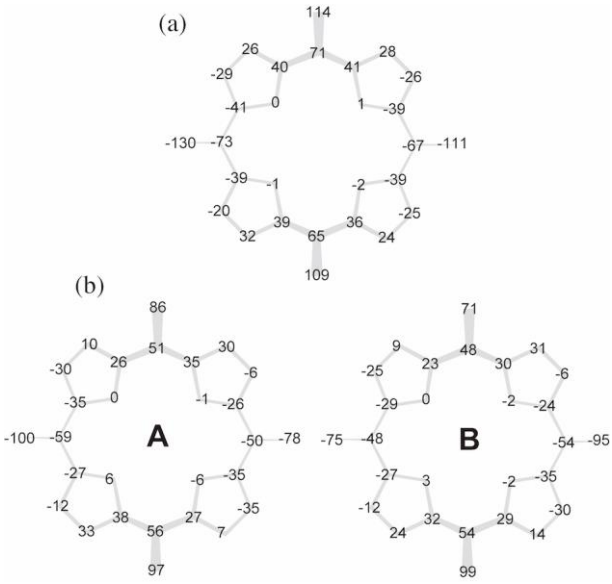

Fig. 4 Comparison of the closed shell tmp ligands. Deviation from the least-squares mean plane determined using the core 24 atoms ($d \times 10^2$ in Å) for tmp in (a) TPP[Co(tmp)$(CN)_2$]·1/2(acetone)·H_2O and (b) {[Co(tmp)(CN)](acetone)}$_n$.

Structures of crystals with open shell tmp ligands

Co(tmp)$(CN)_2$. One Co(tmp)$(CN)_2$ unit is crystallographically independent, and there are inversion centers between the Co(tmp)$(CN)_2$ units. As mentioned later, the tmp is open shell, and it is in the ruffled form as observed for the closed shell tmp. The tmp rings form slipped stacks along the [100], [011], and [01-1] directions, resulting in three-dimensional π–π interactions (Fig. 5a). Details of the π–π interactions are discussed in the next section.

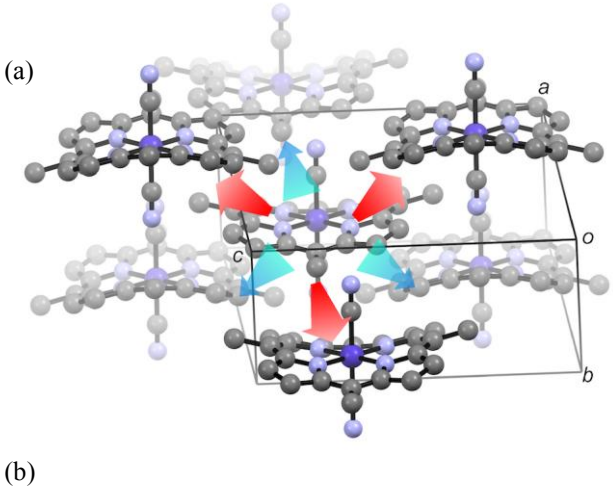

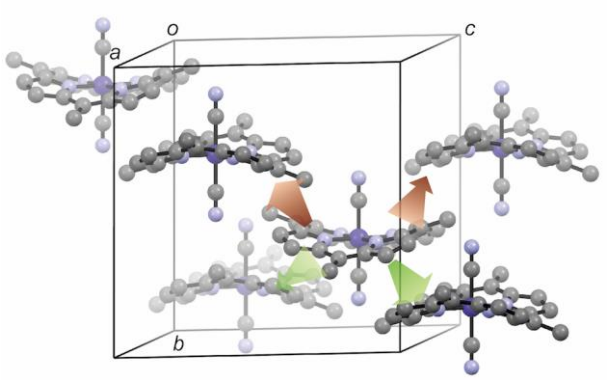

Fig. 5 (a) Perspective view of the unit cell of $Co(tmp)(CN)_2$ and (b) perspective view of the unit cell of $Co(tmp)(CN)_2 \cdot 2CH_3CN$. For clarity, CH_3CN molecules are omitted. Red and blue arrows in (a) and green and brown arrows in (b) indicate the π–π interactions (see Fig. 8).

$Co(tmp)(CN)_2 \cdot 2CH_3CN$. The NC-Co-CN axis coincides with the two-fold axis, and one-half of the $Co(tmp)(CN)_2$ unit is crystallographically independent. Again, the tmp ring is deformed in the ruffled form (Fig. 5b). There are two types of π–π interactions, with one along the [001] direction and the other along the [101] direction. Both form zigzag networks. Combination of these π–π interactions forms π–π networks along the [112] and [1-12] directions. Two CH_3CN molecules arranged in an antiparallel fashion are located in the space formed by six $Co(tmp)(CN)_2$ units.

ESR of $Co(tmp)(CN)_2$. The cyclic voltammogram of $TPP[Co^{III}(tmp)(CN)_2] \cdot 1/2(acetone) \cdot H_2O$ indicated reversible oxidation processes at relatively low potentials (the 1st oxidation potential E_{1st}^{ox} = 0.72 V vs. SCE in acetonitrile; Fig. S2 in the ESI†). Among the components of the TPP salt, oxidation is considered to exclusively occur in the tmp^{2-} π-ligand, since the other components are hardly oxidized. This point was confirmed by observing the ESR spectrum of $Co(tmp)(CN)_2$. Fig. 6 shows the ESR spectra of $Co(tmp)(CN)_2$, $Co^{II}(tmp)$, and $TPP[Co^{III}(tmp)(CN)_2] \cdot 1/2(acetone) \cdot H_2O$. $Co(tmp)(CN)_2$ shows a sharp signal at g = 2.00 with the line width of 41 G (typical π-radical), while there is no signal for the TPP salt (before the electrolysis; non-magnetic d^6 Co^{III}) and a broad signal at g = 2.49 for $Co^{II}(tmp)$ (signal from d^7 Co^{II} (S = 1/2); Fig. S3 in the ESI†). From these data, it is reasonable to assign $Co(tmp)(CN)_2$ as a typical π-radical (tmp^{2-} is oxidized to tmp^{1-}

anion radical). Since the net charge of the molecular unit is neutral ($Co^{3+}(tmp^{1-})(CN^{-})_2$), we refer $Co(tmp)(CN)_2$ as a neutral radical.

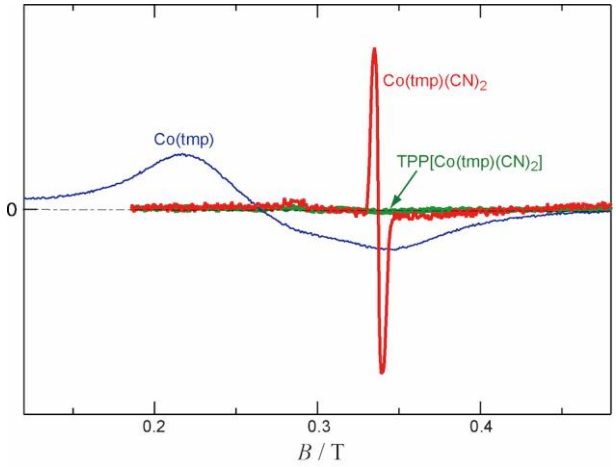

Fig. 6 ESR spectra of $Co(tmp)(CN)_2$, $Co^{II}(tmp)$, and $TPP[Co^{III}(tmp)(CN)_2]\cdot 1/2(acetone)\cdot H_2O$. Modulation amplitude and receiver gain for $Co^{II}(tmp)$ were amplified compared with the other two samples.

SOMO of $Co(tmp)(CN)_2$ neutral radical. We define the HOMO as the next occupied MO of the SOMO (Fig. 7a). Molecular orbital calculations using extended Hückel methods gave a_{2u}-SOMO and a_{1u}-HOMO for both neutral radical crystals (Fig. 7b). The energy difference between the SOMO (-11.40 eV) and HOMO (-11.57 eV) was rather small in $Co(tmp)(CN)_2$, and, also in $Co(tmp)(CN)_2\cdot 2CH_3CN$ (SOMO = -11.34 eV, HOMO = -11.58 eV). Such small energy differences between the SOMO and HOMO suggest that both orbitals may contribute to intermolecular charge transfer (CT). This situation is similar to the case of CT complex formation of $H_2(tmp)$, where both of the energetically close orbitals (a_{2u}- and a_{1u}-type HOMO and the next-HOMO) nearly equally contributed to the CT interactions with 7,7,8,8-tetracyanoquinodimethane-type acceptors.[25]

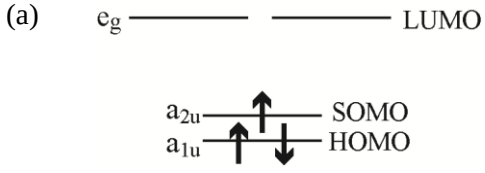

(b)

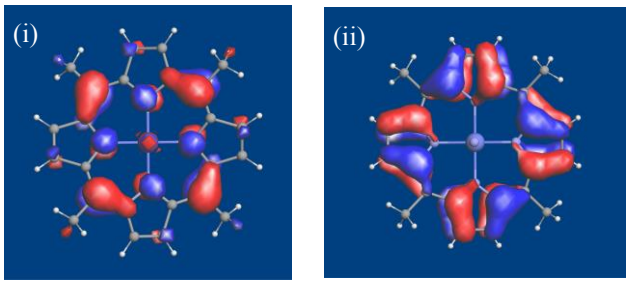

Fig. 7 (a) Energy level diagram and (b) molecular orbitals of (i) SOMO (a_{2u}) and (ii) HOMO (a_{1u}) of the Co(tmp)$(CN)_2$ neutral radical.

Based on these results, overlap integral values between SOMOs, between HOMOs, and between the SOMO and HOMO were calculated (Fig. 8). For the Co(tmp)$(CN)_2$ crystal, the overlap integrals were evaluated between a central molecule and six different neighboring molecules. The values were rather small with a range of 0.1–2.8 × 10^{-3}. The difference in the values between SOMOs, between HOMOs, and between the SOMO and HOMO was small. Therefore, in this crystal, both a_{2u}-SOMO and a_{1u}-HOMO probably contribute to the intermolecular π–π interactions. The situation in the Co(tmp)$(CN)_2$·2CH_3CN crystal is similar. The overlap integral values between SOMOs, between HOMOs, and between the SOMO and HOMO were similar, suggesting nearly equal contribution of a_{2u}-SOMO and a_{1u}-HOMO to the intermolecular π–π interactions.

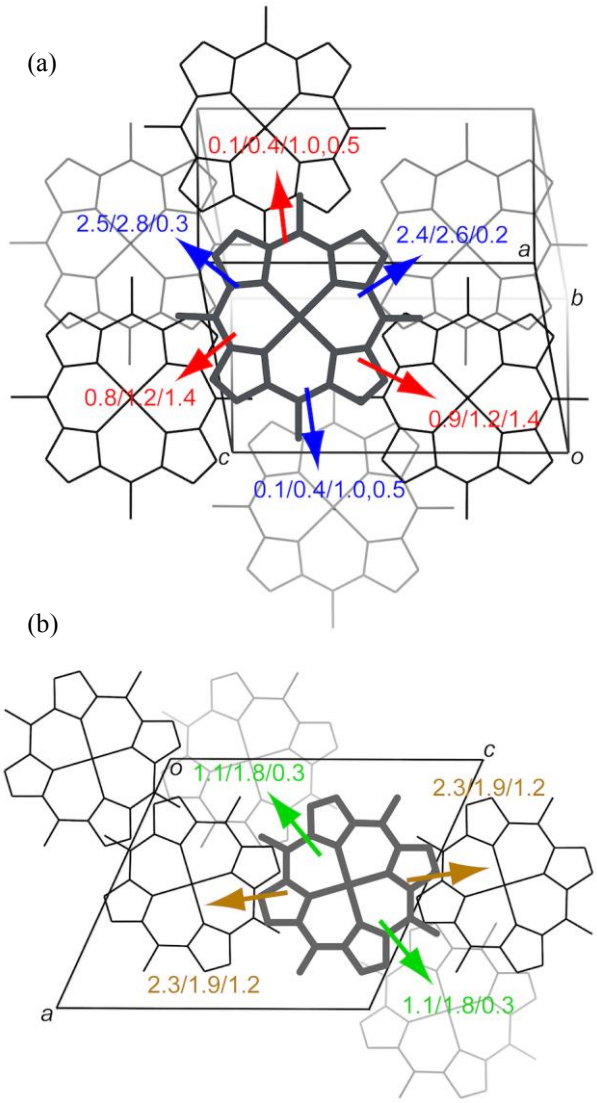

Fig. 8 Overlap integral values (SOMO–SOMO/ HOMO–HOMO/ SOMO–HOMO; all values are $\times 10^3$) (a) between the central radical molecule and six coordinating molecules in Co(tmp)$(CN)_2$ (shown in Fig. 5a), and (b) between the central radical molecule and four coordinating molecules in Co(tmp)$(CN)_2 \cdot 2CH_3CN$ (shown in Fig. 5b).

Molecular structure of open shell tmp. The distances from the least-squares mean plane to the meso carbons are shown in Fig. 9. The average values of the absolute distances for the meso carbons were 0.52 Å in Co(tmp)$(CN)_2$ and 0.67 Å in Co(tmp)$(CN)_2 \cdot 2CH_3CN$. The ruffled deformation of the open shell tmp was similar to that observed for the closed shell tmp. Similar ruffled deformation was reported for the

face-to-face stacked one-dimensional partially oxidized salts of $[Ni^{II}(tmp)]_2PF_6$ and $Ni^{II}(tmp)I$,[14,15] with average values of the absolute distances for the meso carbons of 0.29 and 0.28 Å, respectively. The cause of the larger ruffled deformation of the $Co^{III}(tmp)(CN)_2$ unit compared with that of $Ni^{II}(tmp)$ was probably the difference in the ionic radius (Co^{III} : 0.63 Å, Ni^{II} : 0.69 Å). Indeed, most of the porphyrin complexes with Co^{II} central metal (ionic radius: 0.72 Å) were found to be planar or slightly deformed.[26–30] However, most of the porphyrin complexes with Co^{III} central metal were reported to be largely deformed in ruffled forms.[31–33] It should be noted that this trend, smaller central metal leads to larger deformation of the pophyrinato ligand, is a rough view. The central metal size may be only one of the factors that deform the porphyrinato ligand, and some (porphyrinato)cobalt complexes do not follow this tendency probably due to the packing forces.

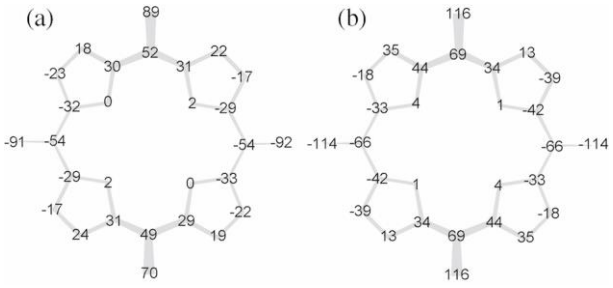

Fig. 9 Comparison of the open shell tmp ligands. Deviation from the least-squares mean plane determined using the core 24 atoms ($d \times 10^2$ in Å) for tmp in (a) $Co(tmp)(CN)_2$ and (b) $Co(tmp)(CN)\cdot 2CH_3CN$.

Optical and Charge Transport Properties

Optical properties. In the diffuse reflectance spectra shown in Fig. 10, two neutral radical crystals showed an additional absorption band at 1.4–1.5 eV compared with the closed shell TPP salt. Since this band is absent in the solution spectrum of the neutral radical $Co(tmp)(CN)_2$ (Fig. 10a), the additional band observed for the neutral radical crystals may be attributed to intermolecular CT between the open shell tmp ligands.

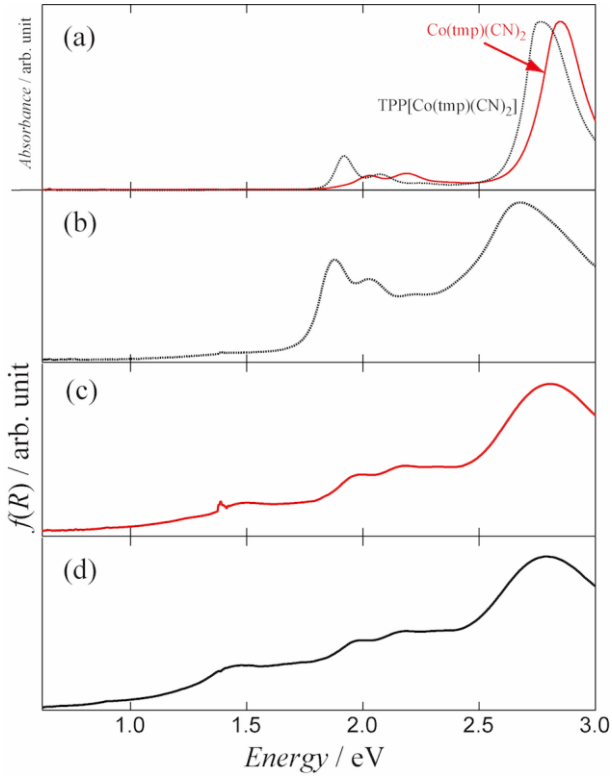

Fig. 10 Vis-NIR spectra of the CH_3CN solution of TPP[Co(tmp)$(CN)_2$] and Co(tmp)$(CN)_2$ (a), diffuse reflectance spectra of (b) TPP[Co(tmp)$(CN)_2$]·1/2(acetone)·H_2O, (c) Co(tmp)$(CN)_2$, and (d) Co(tmp)$(CN)_2$·$2CH_3CN$. The reflectance spectra were converted to the Kubelka-Munk function $f(R)$.

Charge transport properties. Both the neutral radical crystals showed room temperature resistivity of about 10^6 Ω cm (Fig. 11). The activation energy, E_a, of conduction was 0.31 eV for Co(tmp)$(CN)_2$ and 0.29 eV for Co(tmp)$(CN)_2$·$2CH_3CN$. In both radical crystals, π–π interactions are extended three-dimensionally with nearly isotropic overlap integrals. The energy bands originated from the SOMOs and HOMOs for the neutral radical crystals are expected to be extremely narrow due to the small π–π overlaps between the tmp rings. In this situation, the charge transport is regulated by the electron correlation energy. Therefore, the origin of E_a may be assigned to the electron correlation energy on-site of the tmp ring and between the tmp rings. This situation is in common with the neutral radical Pc crystals of Co(Pc)$(CN)_2$, in which the overlap integral values are small, typically 1–5 × 10^{-3} for the Pc π–π stacks, due to the slipped stacking.[5] They also showed thermally activated conduction, and the origin is assumed

to be the electron correlation. As a unique point of the Pc system, the room temperature resistivity was found to be changed following the dimensionality of the π–π network. When the π–π interaction was almost negligible, the room temperature resistivity was about 10^4 Ω cm, whereas for the system with appreciable one-dimensional π–π interactions, it was 10^2–10^3 Ω cm, When the π–π network was two-dimensional, the room temperature resistivity was 10^0–10^2 Ω cm, whereas it was 10^0–10^1 Ω cm for the three-dimensional system.[34] Compared with the Pc system, the $Co(tmp)(CN)_2$ neutral radical crystals showed much higher room temperature resistivity despite their comparable π–π overlap integrals. This suggests that the electron correlation energy is larger in the tmp system than in the Pc system.

By comparison, the room-temperature resistivity of the CN-bridged polymer was rather high (10^8 Ω cm), with an activation energy of about 0.5 eV. Because the tmp ring was not oxidized, there were no charge carriers. In addition, the π–π interactions in the crystal were negligible. Therefore, the high resistivity is considered to be reasonable.

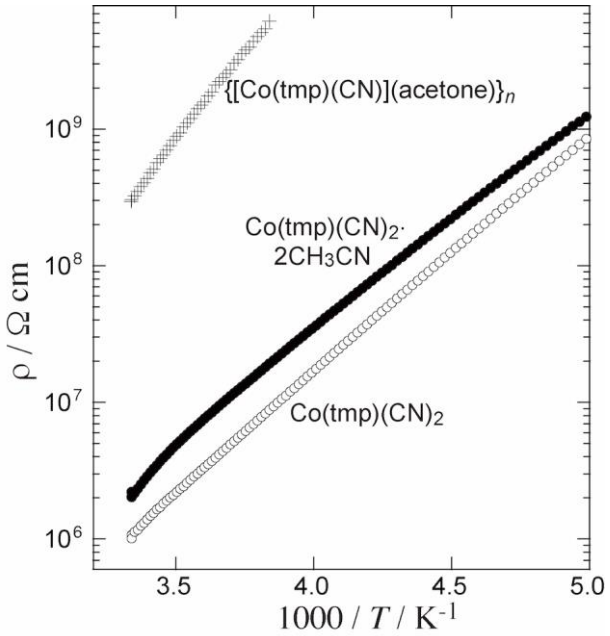

Fig. 11 Temperature dependence of the resistivity of single crystals of $\{[Co(tmp)(CN)](acetone)\}_n$, $Co(tmp)(CN)_2 \cdot 2CH_3CN$, and $Co(tmp)(CN)_2$.

Conclusions

An axially ligated Co(tmp) anion, $[Co^{III}(tmp)(CN)_2]^-$, was prepared and subjected to electrochemical oxidation. As a result, the solvent-free and solvent-inclusive neutral radical crystals were obtained. When acetone was used as the solvent, single crystals of

the CN-bridged polymer of $\{[Co^{III}(tmp)(CN)](acetone)\}_n$ were obtained as a byproduct. The π–π interactions between the closed shell tmp rings were negligible, and the resistivity was very high. This suggests that the ⋯Co–CN–Co–CN–Co⋯ polymer backbone itself does not contribute to the charge transport. Therefore, relatively high electrical conductivity reported for $[Co(Pc)(CN)]_n$[35] may result from some inter-polymer π–π interactions.

In both radical crystals, the π–π interactions involved both the SOMO and HOMO. The high resistivity indicates larger electron correlation in the tmp system than in the Pc system, and that reduction of the macrocycle size is effective to enhance electron correlation. Replacement of the central metal with magnetic ions is therefore expected to induce enhanced magnetotransport effects, and the study is in progress.

Acknowledgements

This work was supported in part by a Grant-in-Aid for Scientific Research from Japan Society for the Promotion of Science (KAKENHI Grant No. 26288029), and Japan Science and Technology Agency, CREST. The authors thank Dr. A. Kobayashi (Hokkaido Univ.) for access to a Bruker D8 ADVANCE powder X-ray diffractometer.

References

1 *Phthalocyanines: Properties and Applications*, eds. C. C. Leznoff and A. B. P. Lever, Wiley-VCH, Cambridge, 1989–1996; Vol. 1–4.

2 G. H. Heilmeier and S. E. Harrison, *Phys. Rev.*, 1963, **132**, 2010–2016.

3 C. S. Schramm, R. P. Scaringe, D. R.Stojakovic, B. M. Hoffman, J. A. Ibers and T. J. Marks, *J. Am. Chem. Soc*., 1980, **102**, 6702–6713.

4 T. Inabe and H. Tajima, *Chem. Rev*., 2004, **104**, 5503–5533.

5 T. Inabe, *J. Porphyrins Phthalocyanines*, 2001, **5**, 3–12.

6 H. Hasegawa, T. Naito, T. Inabe, T. Akutagawa and T. Nakamura, *J. Mater. Chem*., 1998, **8**, 1567–1570.

7 M. Matsuda, T. Naito, T. Inabe, N. Hanasaki and H. Tajima, *J. Mater. Chem*., 2001, **11**, 2493–2497.

8 D. E. C. Yu, M. Matsuda, H. Tajima, A. Kikuchi, T. Taketsugu, N. Hanasaki, T. Naito and T. Inabe, *J. Mater. Chem*., 2009, **19**, 718–723.

9 M. Ishikawa, T. Asari, M. Matsuda, H. Tajima, N. Hanasaki, T. Naito and T. Inabe, *J. Mater. Chem*., 2010, **20**, 4432–4438.

10 M. Matsuda, T. Naito, T. Inabe, N. Hanasaki, H. Tajima, T. Otsuka, K. Awaga, B. Narymbetov and H. Kobayashi, *J. Mater. Chem*., 2000, **10**, 631–636.

11 N. Hanasaki, H. Tajima, M. Matsuda, T. Naito and T. Inabe, *Phys. Rev. B*, 2000, **62**, 5839–5842.

12 N. Hanasaki, K. Masuda, K. Kodama, M. Matsuda, H. Tajima, J. Yamazaki, M. Takigawa, J. Yamaura, E. Ohmichi, T. Osada, T. Naito and T. Inabe, *J. Phys. Soc. Jpn*., 2006, **75**, 104713.

13 H. Tajima, G. Yoshida, M. Matsuda, K. Nara, K. Kajita, Y. Nishio, N. Hanasaki, T. Naito and T. Inabe, *Phys. Rev. B*, 2008, **78**, 064424.

14 L. J. Pace, J. Martinsen, A. Ulman, B. M. Hoffman and J. A. Ibers, *J. Am. Chem. Soc*., 1983, **105**, 2612–2620.

15 T. P. Newcomb,; M. R. Godfrey, B. M. Hoffman and J. A. Ibers, *J. Am. Chem. Soc*., 1989, **111**, 7078–7084.

16 T. P. Newcomb, M. R. Godfrey, B. M. Hoffman, J. A. Ibers, *Inorg. Chem*., 1990, **29**, 223–228.

17 S. Neya and N. Funasaki, *J. Heterocyclic Chem*., 1997, **34**, 689–690.

18 C. Shi and F. C. Anson, *Inorg. Chem*., 1998, **37**, 1037–1043.

19 B. C. Chow and I. A. Cohen, *Bioinorg. Chem*., 1971, **1**, 57–63.

20 G. M. Sheldrick, *Acta Crystallogr., Sect A*, 2008, **64**, 112–122.

21 J. Ren, W. Liang and M.-H. Whangbo, *CAESAR*; Prime-Color Software, Inc.: Raleigh, NC, 1998.

22 M. Hanack and M. Lang, *Adv. Mater*., 1994, **6**, 819–833.

23 M. Hanack, A. Datz, R. Fay, K. Fischer, U. Keppeler, J. Koch, J. Metz, M. Mezger, O. Schneider and H. –J. Schulze, *Handbook of Conducting Polymers*, ed. T. A. Skotheim, Marcel Dekker, New York, 1986.

24 S. Takano, T. Naito and T. Inabe, *J. Mater. Chem*., 1998, **8**, 511–513.

25 J. F. F. Jose-Larong, Y. Takahashi and T. Inabe, *Struct. Chem*., 2013, **24**, 1113–1222.

26 B, F. O. Nascimento, M. Pineiro, A. M. d'A. R. Gonsalves, M. R. Silva, A. M. Beja and J. A. Paixao, *J. Porphyrins Phthalocyanines*, 2007, **11**, 77–84.

27 W. R. Scheidt, *J. Am. Chem. Soc*., 1974, **96**, 84–89.

28 W. Chen and S. Fukuzumi, *Eur. J. Inorg. Chem*., 2009, 5494–5505.

29 R. G. Little, J. A. Ibers, *J. Am. Chem. Soc.*, 1974, **96**, 4440–4446.

30 W. R. Scheidt and I. Turowska-Tyrk, *Inorg. Chem*., 1994, **33**, 1314–1318.

31 Y. Iimura, T. Sakurai and K. Yamamoto, *Bull. Chem. Soc. Jpn*., 1988, **61**, 821–826.

32 H. Masuda, T. Taga, K. Osaki, H. Sugimoto and M. Mori, *Bull. Chem. Soc. Jpn*., 1982, **55**, 4–8.

33 Y. Belghith, J.-C. Daran and H. Nasri, *Acta Crystallogr., Sect. E: Struct. Rep. Online*, 2012, **68**, m1104–m1105.

34 T. Inabe, M. Ishikawa, T. Asari, H. Hasegawa, A. Fujita, N. Matsumura, T. Naito, M. Matsuda and H. Tajima, *Mol. Cryst. Liq. Cryst*., 2006, **455**, 87–92.

35 J. Metz and M. Hanack, *J. Am. Chem. Soc*., 1983, **105**, 828–830.